Trop J Nat Prod Res, November 2025; 9(11): 5608 – 5620

ISSN 2616-0684 (Print)
ISSN 2616-0692 (Electronic)

Tropical Journal of Natural Product Research

Available online at https://www.tjnpr.org

Original Research Article

Biosynthesis, Characterization, and Antihyperlipidemic Property of Green Silver Nanoparticles Derived from *Borassus aethiopum* Hypocotyl Extract in Poloxamer 407-Induced Hyperlipidemic Pre-Clinical Models

Moses D. Adams[1]* and Judith N. Ohanaka[2]

[1]*Clinical Biochemistry, Phytopharmacology and Biochemical Toxicology Research Laboratory (CBPBT-RL), Department of Biochemistry, Baze University, Abuja 900108, Nigeria*
[2]*Department of Biochemistry and Biotechnology, Faculty of Science, Nile University of Nigeria*.

ARTICLE INFO

Article history:
Received 16 August 2025
Revised 01 November 2025
Accepted 12 November 2025
Published online 01 December 2025

Copyright: © 2025 Adams and Ohanaka. This is an open-access article distributed under the terms of the Creative Commons Attribution License, which permits unrestricted use, distribution, and reproduction in any medium, provided the original author and source are credited.

ABSTRACT

The use of silver nanoparticles (AgNPs) for hyperlipidemia is advancing nanocardiology research owing to their nano-size, targeted therapy, biomembrane penetrating ability and easy delivery. This study synthesized, characterized, and assessed the antihyperlipidemic potential of AgNPs derived from the aqueous extract of *Borassus aethiopum* hypocotyl (BAHAE) in poloxamer-407-induced hyperlipidemic rats. Thirty-five rats were divided into seven groups (n=5). Animals in Group A received distilled water (DW). Animals in Group B-G, which were induced into hyperlipidemia with poloxamer-407 (300 mg/kg BW), received DW, fenofibrate [standard medication] (250 mg/kg BW), 10 mg/kg BW nano-sized particles (NSP), 20 mg/kg BW NSP, 200 mg/kg BW of BAHAE, and 400 mg/kg BW of BAHAE, respectively. Treatment occurred for 14 days. Related bioassays and characterization were conducted using standard protocols. Poloxamer-407 which substantially *($p<0.05$)* lowered HDLC, CAT, SOD, and GPx, significantly elevated serum levels of CK-MB, cTnI, LDH, MDA, TC, TAG, and LDLC. BAHAE and AgNPs restored the examined biomarkers, with profound effect from AgNPs than from BAHAE or fenofibrate. UV-Vis spectroscopy confirmed the synthesized AgNPs peak at 205 nm. FTIR indicated peaks/functional groups that are involved in the synthesis and stabilization of AgNPs, with a prominent peak at 991.5;79.4 wavelength/intensity. While XRD showed an amorphous/nanocrystalline structure with four intense peaks at 2θ angles of 19.01°, 31.10°, 37.50°, and 46.20°, SEM-EDX showed a rough and irregular surface with agglomerated particles. EDXRF spectrum showed the most prominent peak at ~22.16 keV. AgNPs normalized the poloxamer-407-induced hyperlipidemic alterations in rats and could be explored in the management of hyperlipidemia.

Keywords: *Borassus aethiopum*, Hyperlipidemia, Green silver nanoparticles, Poloxamer-407, Cardiac troponin I, Creatine kinase, Scanning electron microscopy.

Introduction

Hyperlipidemia is a clinical state characterized by elevated level of lipids (including cholesterol and triglycerides) in the extracellular fluid. The condition initially presents with elevated systolic and diastolic heart movement followed by increased risk of hypertension, stroke, and other cardiac-related diseases, all owing to an alteration in normal blood movement through the arteries.[1] Hyperlipidemia is classified into two major types: primary (genetic) and secondary (acquired) hyperlipidemia.

*Corresponding author .Email: mdadamsonline@gmail.com
Tel.: +234 8038952634.

Citation: Adams MD and Ohanaka JN. Biosynthesis, Characterization, and Antihyperlipidemic Property of Green Silver Nanoparticles Derived from *Borassus aethiopum* Hypocotyl Extract in Poloxamer 407-Induced Hyperlipidemic Pre-Clinical Models. Trop J Nat Prod Res. 2025; 9(11): 5608 – 5620 https://doi.org/10.26538/tjnpr/v9i11.48

Official Journal of Natural Product Research Group, Faculty of Pharmacy, University of Benin, Benin City, Nigeria

The primary hyperlipidemia (familial hyperlipidemia) is mainly passed-on via genetic disorders and this include hypercholesterolemia (inherited LDLC), hypertriglyceridemia (inherited TAG), combined hyperlipidemia (inherited LDLC and TAG) and dysbetalipoproteinemia (inherited IDLC) while secondary hyperlipidemia occur via dietary factors including high intake of saturated fatty acid/trans-fat; cholesterol and refined carbs; cholesterol elevating medications; allied clinical conditions: untreated diabetes, kidney disease; life style factors including physical exercise, obesity, and high alcohol intake.[2] In the year 2008, the global prevalence of total rise in cholesterol for adults was observed as 37% (35% for men and 43% for women). A rise in cholesterol level led to 4.4 million deaths every year, or 7.8% of all mortality rates. About 24% of cardiovascular disease (CVD)-related mortality is caused by high LDL cholesterol.[3] The estimate of the WHO on hyperlipidemia is put at Europe (52.6%), America (46.8%), South East Asia (32.7%), and Africa (23.1%).[4,5] The recently introduced Systematic Coronary Risk Evaluation 2 (SCORE2) model presents an estimate of a 12-year risk of severe and non-severe CVD crises in people aged between 41 and 70, thus helping to identify people at high risk of presenting CVD events.[6] Hyperlipidemia is managed and treated by eating a healthy diet, being more physically active, losing weight, and quitting alcohol and smoking.[7] These hyperlipidemic medications lead to side effects like muscle aches, digestive issues, headaches, dizziness, blood sugar levels, liver abnormalities, rhabdomyolysis (muscle breakdown), and allergic reactions.[8,9] Nanoparticles offer significant advantages over conventional hyperlipidemic medications as they easily recognize and bind to specific cell receptors delivering medications to their desired

© 2025 the authors. This work is licensed under the Creative Commons Attribution 4.0 International License

ISSN 2616-0684 (Print)
ISSN 2616-0692 (Electronic)

location, enhancing increased uptake of medications by cells/tissues, prolonged circulation in the bloodstream, delivery of medications to previously inaccessible target locations by overcoming biological barrier/membrane (blood brain barrier-BBB), protecting drugs from enzymatic degradation, improving poorly soluble medications, delivering medications directly to their target site of therapeutic action, bypassing the mechanism of drug resistance especially in cancer treatment, multiple routes of administration, overcoming drug resistance and delivery of medications at a controlled rate which lowers drug fluctuation and risk of toxicity.[10]

Nanotechnology is involved with the manipulation of matter at the molecular and atomic level within the range of 1 to 100 nanometers. It focuses on developing, forming, and utilizing structures, devices, and materials with nanoscale specifications, often leveraging the special physicochemical features that arise at the nanoscale. Nanotechnology spans many disciplines, including biology, pharmacy, engineering, physics, medicine, and chemistry.[11] The characterization of nanoparticles is achieved via biophysical methods, including microscopic (AFM, TEM, SEM, SPM, OM, EM) and spectroscopic (UV-VIS, SS-NMR, PCS, XRD, FTIR, DCS, ICP-MS, XPS, EDX, NTA, DLS, EDXRF). The characterization of particles derived through nanotechnology primarily involves evaluating morphology, crystalline structure, functional group identification, and physicochemical features including shape, elemental composition, size, and surface properties. Nanoparticle characterization is vital for controlling and confirming biosynthesized nanoparticles, optimizing nanomaterials across different disciplines, and understanding nanoparticle properties (size, shape, and composition).[12] *Borassus aethiopum* (Mart.), belongs to the *Aracaceae* family and is mainly known in English as *African Fan Palm*. *B. aethiopum* contains nutrient that supplies energy, making it a staple food consumed in most Northern Nigeria States.[13] Ethnic groups in Nigeria identify the plant by various names; it is commonly identified as *Kemelutu* in Kanuri, *Ubiri* in Igbo, *Muruchi* or *Giginya* in Hausa, and *Agbon Oludu* in Yoruba. It is a typical solitary palm, 25m high and 1m wide at the base. The plant's hypocotyl is ingested raw or boiled and is reported to possess various biological properties in adult males.[14] To the best of our knowledge, reports on the antihyperlipidemic action of *Borassus aethiopum* fruit include those by Aduwamai *et al*[15], who concluded that the methanol fruit extract of *Borassus aethiopum* displayed potent cholesterol-lowering property when compared with atorvastatin (standard cholesterol-lowering medication), as well as Maniru *et al*[16], who reported that the fruit extract of *B. aethiopum* is healthy/safe for consumption and for reduction of BMI and other lipid biomarkers. These studies focused only on the lipid-lowering effect of the fruit extract of *B. aethiopum* in rats, with no information on the enormous benefits of the nanosized materials derived from the plant hypocotyl, creating a research gap yet to be addressed. Therefore, in this study, we biosynthesized green silver nanoparticles from *Borassus aethiopum* hypocotyl extract, characterized the synthesized nanoparticles, and examined the antihyperlipidemic activity of the synthesized AgNPs in poloxamer-407-induced hyperlipidemic animals.

Materials and Methods

Plant and its identification

Fresh hypocotyl of *B. aethiopum* Mart., family, *Aracaceae* was collected, on request, from local herb vendors, at Jere (Global Positioning System, GPS: Latitude: 09º34'08"N Longitude: 07º26'06"E), along the axis of Kaduna Road of the Kagarko LGA of Kaduna State, Nigeria. It was confirmed at the Herbarium and Ethnobotany Unit of the National Agency for Pharmaceutical Research and Development (NIPRD), Abuja, Nigeria, where a Voucher Sample Number (NIPRD/H/7257) was assigned. The hypocotyl of *Borassus aethiopum* (Mart.) was further confirmed at http://www.theplantlist.org/tpl1.1/ on September 15, 2024, and is known to be error-free.

Animal models

Thirty-five healthy male *Rattus norvegicus* (Wistar strain; mean age and mass: 10 weeks 8 days and (90.28 – 120.35 g) from various husbandry were picked from the Veterinary Teaching Hospital, University of Abuja (UniAbuja), Abuja, Nigeria. The animals were arranged in 10 rectangular-shaped laboratory polypropylene rat cages (Type 2; Rara Pharmatech and Surgical Ltd, Ahmedabad, Gujarat, India) with dimensions of 430 × 285 × 155 mm (L × B × H) and a ground spacing of 945 cm^2. The animals were kept within the same Veterinary Hospital Facility, where specified housing environmental conditions (temperature: 27 ± 3◦C; photoperiod: 11 h light/dark cycle; and relative humidity: 50–57 %) were maintained. The animals were allowed to feed freely on pelletized food (Chidex Feeds, a product of Chidex Poultry Farm, Jikwoyi, Abuja, Nigeria) and clean water.

Test kits and chemical agents

Assay kits for the determination of serum levels of TC, HDL-C, LDL-C, TAG, and LDH were factory-made products obtained from Gentex Pharmaceutical Co., Huitai, Thailand. All other chemicals or reagents used in the study were obtained from Sigma-Aldrich (Canada) Ltd., Oakville, Ontario, Canada.

Ethics approval

This study was conducted based on an Ethical Clearance obtained from the University of Abuja Ethics Committee on Animal Use with Reference Number: UAECAU/2024/022.

Preparation of aqueous extract of Borassus aethiopum hypocotyl

The method previously used by Adams and Eze[17] was adopted with slight modifications. Briefly, the *Borassus aethiopum* hypocotyl was shade-dried and thereafter ground to powder using a grinding machine. A known quantity (500 g) of the powdered hypocotyl was dissolved in 2.5 L of distilled water (DW) for 75 hours in a well-sealed container. The extract was separated from the residue with a Sieve (Labbazaar Test Sieve, 90 Microns) and concentrated in a steam bath. This step was repeated several times until a crude aqueous extract (22.46 g) was obtained. A portion of the extract was redissolved in DW to produce the doses of 200 and 400 mg/kg BW needed for the study.

Synthesis of green silver nanoparticles from aqueous extract of Borassus aethiopum hypocotyl

The synthesis of green AgNPs was carried out as previously described, with minor modifications.[18] The dried aqueous hypocotyl extract was ground into powder. A known quantity (5 g) of the powdered sample was dissolved in 100 mL of DW and allowed to stand overnight with constant stirring using a magnetic stirrer to ensure proper dissolution. The mixture was separated with Whatman Filter Paper to obtain a filtrate and residue. The filtrate was purified using a Suction Pumping Machine to get a pure solution. A known quantity (50 mL) of the purified solution was mixed with 100 mL of silver nitrate wrapped in foil paper. The solution was allowed to stand for 24 hours. Thereafter, a colour change from light brown to deep brown was observed, indicating the synthesis of nanoparticles. The solution was then centrifuged at 2000 g for 10 minutes to separate the solution from the particles. The supernatant was discarded to obtain the green silver nanoparticles (AgNPs). The nanoparticles were then stored in a sterile sample bottle and labeled for further use. In order to break-up the AgNP clusters and ensure a uniform suspension, the nanoparticles were first dissolved with dimethyl sulfoxide (DMSO) and thereafter sonicated using a standard sonication protocol (via an ultrasonic bath, by maintaining constant temperature). The dissolved particles were then dissolved with water to give the required doses of 10 and 20 mg/kg BW NSP used in the study.

Animal grouping for in vivo antihyperlipidemic study

In accordance with the ethical provisions and laboratory guidelines provided by Baze University, Abuja, and the UAECAU ethical committee (Ethical Reference Number: UAECAU/2024/022), adequate care was taken to house the animals. Wistar rats (35) were assigned to seven groups (A-G; n = 5/group) as shown below:

Group A: Healthy rats + DW only (Sham Control)
Group B: Hyperlipidemic rats + DW
Group C: Hyperlipidemic rats + fenofibrate (250 mg/kg BW)
Group D: Hyperlipidemic rats + Nanosized AgNPs (10 mg/kg BW)

© 2025 the authors. This work is licensed under the Creative Commons Attribution 4.0 International License

Group E: Hyperlipidemic rats + Nanosized AgNPs (20 mg/kg BW)
Group F: Hyperlipidemic rats + BAHAE (200 mg/kg BW)
Group G: Hyperlipidemic rats + BAHAE (400 mg/kg BW)

To achieve proper dissolution of the AgNPs, sonication was carried out, followed by filtration. The animals received oral gavage of the AgNPs and BAHAE once daily for 14 days. The selection of doses for AgNPs and BAHAE was guided by information obtained from an ethnobotanical survey on the local folklore use of the plant hypocotyl.

Preparation of serum

The experimental animals were anesthetized using diethyl ether, and the fur hair was quickly removed from the neck region of the animal after which the jugular veins were cut open with an aseptic blade where blood cells (6 mL) were collected into plain blood sample container and this was centrifuged at 1500 *g* x 15 min with a BioBase Laboratory Centrifuge (Model BD900B, BioBase Scientific {Shandong} Co., Ltd., Jinan, Shandong, China). Serum (supernatant) was carefully pipetted using a dropper and then used for selected hormone, enzyme, and biochemical assays.

Determination of selected serum biomarkers

The determination of the selected serum biomarker levels/activity followed procedures previously reported: TC, HDLC, LDLC, TAG, MDA, CAT, SOD, GP_x.[19-26]

Determination of serum cardiac troponin I and some related enzyme markers

Estimation of serum cardiac troponin I (cTnI) concentration

The previously described protocol, with slight modifications, was used to assess cardiac troponin I serum concentration in the experimental animals.[27,28] In brief, the i-STAT cTnI test pack, which uses a two-sided enzyme-linked immunosorbent assay (ELISA) protocol, was used. Antibodies designed explicitly for human cardiac troponin I (cTnI) are found on the electrochemical detecting knob on the silicon splint. The other segment of the silicon chip was equipped with an alkaline phosphatase (ALP) antibody conjugate that binds to a different segment of the cTnI solution. The serum was mixed with the sensor to allow dissolution of the sample with the enzyme conjugate. The cTnI in the sample was tagged with ALP, adsorbed to the surface of the electrochemical detector, and incubated for 5 minutes. The sample containing the higher enzyme conjugate was washed to remove the detecting sensor. The enzyme bound to the antigen-antibody complex cleaves the substrate, generating an electrochemical detection product (EDP). The generated EDP was then used to measure the cTnI activity in the sample.

Estimation of serum creatine kinase (CK-MB) activity

The procedures described by Gerhardt *et al*.[29] and Rchid *et al*.[30] were used to estimate serum creatine kinase (CK-MB) activity. The process involves incubating 50 µL of the serum with 500 µL of the working solution at 370 °C for 10 minutes. The two solutions were mixed and incubated for 5 minutes at 37°C to react with the CK-MB in the sample, producing a measurable product. The rate of product formation, which is directly proportional to CK-MB activity, is then determined by monitoring absorbance changes at 365 nm with a BioBase Spectrophotometer (Model: BT-UV3951; BioBase Group Manufacturers, Zhangqiu, Shandong, China).

Estimation of serum lactate dehydrogenase (LDH) activity

The methodology described by Glowacka *et al*.[31] was used to measure the animals' serum LDH activity. Serum lactate was measured using an L-lactate testing kit. In a reaction catalyzed by lactate oxidase, oxygen combines with L-lactate in the serum to yield hydrogen peroxide and pyruvate. Thereafter, the generated hydrogen peroxide combined with N-ethyl-N-(2-hydroxy-3-sulphopropyl) m-toluidine and 4-aminoantipyrine in a reaction mediated by peroxidase to produce water and a purple solution. The optical activity of the purple compound was determined with a BioBase Spectrophotometer (Model: BT-UV1901; BioBase Group Manufacturers, Zhangqiu, Shandong, China). A known volume (10 µL) of serum was added to 2000 µL of reagent that contains peroxidase, N-ethyl-N-(2-hydroxy-3-sulphopropyl) m-toluidine, lactate oxidase, and 4-aminoantipyrine. This mixture was incubated at 27°C for 15 minutes for absorbance measurement at 570 nm.[32] The optical activity of the absorbance of the standard solution and serum was then computed against a reagent blank within 20 min after incubation. The standard lactate concentration in the testing kit was 38.20 mg/dL, which was subsequently converted to U/L.

Characterization of synthesized silver nanoparticles

UV–visible (UV-Vis) spectroscopy

The synthesized green AgNPs were characterized using a Shimadzu UV-1900 UV-Vis Spectrophotometer (Model: BT-UV1901; Shanghai, China). The operation of UV radiation typically involves specialized light-emitting diodes (LEDs) that emit UV radiation at specific wavelengths. The device was set at an appropriate wavelength range and intensity of 200-800nm and 1.5 – 6.2 eV, respectively. The UV lamp was positioned at the proper distance from the AgNPs being treated. AgNPs were then exposed to the UV radiation for 10 minutes. The effects of UV radiation on AgNPs were monitored and recorded.

Scanning electron microscopy with energy dispersive X-ray (SEM-EDX) spectroscopy

SEM-EDX spectroscopy of the AgNPs derived from BAHAE was conducted with a scanning electron microscope coupled with an energy dispersive X-ray spectroscopy (Model: PRO: X:805-17934 Phenom World; Serial Number: MVE31580973). The instrument was equipped with three major parts: a sample carrier, an X-ray tube, and an EDX-ray sensor attached to a PC. In brief, the AgNPs were added to the sample carrier and placed in the device for analysis. The X-ray in the cathode ray tube is produced by heating the filament, which emits electrons. Thereafter, the generated electrons were tagged by applying 10 kV to the AgNPs. The initial image of a standard compound microscope displayed on the monitor was sharpened, and the resulting image was then converted to a typical image of a Scanning Electron microscope. Images of the AgNPs were then taken at different magnifications.

X-ray Diffraction (XRD) measurement

A Thermo Fisher X-ray Diffractometer, Scientific Company, Switzerland (Model: ARIL'XTIRAM.X-ray; Serial Number:167482096) was used to analyze AgNPs obtained from BAHAE. An X-ray diffractometer contains three major segments: a sample carrier, an X-ray tube, and an X-ray sensor at an opposite location that spins around the angle of operation. X-rays are produced in a cathode ray tube by heating a filament to generate electrons, accelerating the electrons via application of voltage in the direction of the target, and binding the target substance with the electrons. The tiny film was spotted on the sample carrier and lowered into the device. The left sensor segment was positioned to face the AgNPs at a suitable angle. A high-energy electron subsequently displaced the inner-shell electrons of the AgNPs, generating a typical X-ray spectrum. The intensity of the diffracted X-rays was continuously recorded at different angles using a sensor during XRD of the AgNP. The peak of the intensity was obtained by measuring AgNPs that contain lattice planes with d-spacings appropriate for diffracting X-rays at the value of θ. However, each peak comprises two reflections ($K\alpha_1$ and $K\alpha_2$). At small 2θ values, the $K\alpha_2$ peak overlaps with $K\alpha_1$ and appears as a hump on the $K\alpha_1$ segment. Better separation was obtained at a higher θ value, whereas combined peaks were treated as a single peak. The 2λ position of the diffraction peak was estimated as the midpoint of the peak at 80% of its height. When all the AgNPs had been aspirated, the results were imputed into a PC from the XRD machine. XRD results were presented as peak positions at 2θ, while the X-ray count/intensity was taken as the x-y plot. The intensity (I) was reported as the peak height above background or as the integrated intensity of the peak area. The relative intensity of the AgNPs was calculated as the ratio of the peak intensity to the most intense peak (relative intensity = I/I1× 100).

Fourier transform infrared (FTIR) spectroscopy analysis

An FTIR spectrometer (Model: DW-FTIR-530A) was used to determine the transmission and absorption of infrared radiation by AgNPs. The guiding principle of FTIR is based on differences in chemical interactions within molecules that absorb infrared radiation at

© 2025 the authors. This work is licensed under the Creative Commons Attribution 4.0 International License

ISSN 2616-0684 (Print)
ISSN 2616-0692 (Electronic)

specific frequencies. A known weight (1 g) of the AgNP is placed on the instrument's sample holder. An initial measurement was taken to determine the infrared ray that passes through the empty sample carrier. This preliminary measurement was performed to correct for any initial infrared radiation scattered or absorbed by the sample carrier or the device itself. The FTIR analyzer emits a quantum of infrared radiation that passes through the AgNP, which is then detected by a sensor. The analyzer scanned the AgNPs over a frequency range (4000-400 cm^-1) to measure the amount of radiation transmitted or absorbed by the particles at each frequency. This scan generated a spectrum typical of the AgNPs' absorption pattern. The acquired spectrum was analyzed using Agilent's MicroLab Suite to identify characteristic peaks and patterns. These peaks correspond to the different types of chemical bonds present in the AgNPs, and by comparing the spectrum to a database of known spectra, the chemical composition of the AgNPs was identified. The identified chemical and functional groups were used to determine the type of compound present in the AgNPs, their purity, and the structural properties of the AgNPs.

Energy dispersive X-ray fluorescence (EDXRF) spectrometry analysis
An EDXRF Spectrometer with Model Number: AGIL. QUANIT'X. An EDXRF Analyzer (Serial Number: 9352160; Product Name: Thermo Fisher Scientific Company, Switzerland) was employed to analyze the AgNPs obtained from BAHAE. The instrument had three compartments: a vacuum-pumping device for light metals, helium gas for aqueous samples, and oxygen for light and heavy metals. The dried NPs are first blended into powder using a grinding machine. Thereafter, 2 g of the powdered particles was placed into the sampler carrier (with a polypropylene-thermoplastic bottom) and protected with pieces of cotton wool to prevent it from spraying. The sample carrier containing AgNPs was evacuated for 15 minutes before insertion into the EDXRF spectrometer for elemental analysis. The results obtained for the elemental components of AgNPs were then recorded. A biological calibration method was adopted while the analysis was done in elemental form.

Statistical Analysis
The data were analyzed with one-way (ANOVA) and Duncan Multiple Range Test. Statistical Product and Service Solution, SPSS version 23 (International Business Machines [IBM] Company; Year of Release: 2022) determined that differences at $p<0.05$ were significant.

Results and Discussion

The administration of poloxamer-407 significantly ($p<0.05$) lowered HDLC concentration but elevated serum levels of TC, TAG, and LDLC compared with the distilled water group. However, treatment of the animals with all doses of AgNPs and BAHAE significantly ($p<0.05$) reduced the serum concentrations of LDLC, TC, and TAG, while increasing HDLC levels compared with DW-treated hyperlipidemic animals. The nanoparticles (AgNPs) and extracts (BAHAE) worked in a manner not similar to that of the reference medication (fenofibrate), except for the 200 mg/kg BW of BAHAE, which produced TC values that compared *($p>0.05$)* well with fenofibrate. Treatment of the animals with a 200 dose of BAHAE produced serum HDLC values that compared ($p>0.05$) suitably well with those of the 400 dose of BAHAE (Table 1).

The induction of hyperlipidemia in animals with poloxamer-407 significantly ($p<0.05$) increased the concentration of cTnI and the activities of LDH and CK-MB in the serum of the models when compared with the sham control animals. In contrast, treatment of hyperlipidemic rats with all doses of AgNPs and BAHAE substantially ($p<0.05$) reduced serum cTnI levels and the activities of CK-MB and LDH compared with distilled water-treated hyperlipidemic rats.

Table 1: Effect of *Borassus aethiopum* hypocotyl aqueous extract and green silver nanoparticles on serum lipids (mmol/L) of poloxamer-407 induced hyperlipidemic rats

Treatment Group	TC	TAG	HDLC	LDLC
NR + DW	92.49±3.86^{a}	142.35±4.68^{a}	242.75±6.78^{a}	198.59±4.26^{a}
HR + DW	128.76±5.25^{b}	226.36±5.27^{b}	133.68±3.85^{b}	214.75±5.05^{b}
HR + Fenofibrate	85.26±3.14^{c}	112.42±3.75^{c}	165.26±2.42^{c}	204.72±5.28^{c}
HR + 10 mg/kg body weight of NSP	52.07±2.78^{d}	89.55±2.08^{d}	204.75±5.24^{d}	156.24±3.47^{d}
HR + 20 mg/kg body weight of NSP	67.38±2.94^{e}	85.71±2.62^{e}	209.08±5.38^{e}	168.76±3.25^{e}
HR + 200 mg/kg body weight of BAHAE	86.94±3.48^{c}	104.29±3.86^{f}	192.42±3.45^{f}	182.74±3.98^{f}
HR + 400 mg/kg body weight of BAHAE	72.25±3.52^{f}	98.79±4.72^{g}	190.35±3.36^{f}	191.38±4.63^{g}

Results are the average value ± SEM of five estimations. Superscripted values that show results different from their corresponding reference value, down the column, are significantly different ($p<0.05$)
NR = Normal Rats; **HR** = Hyperlipidemic Rats; **DW =** Distilled Water; **NSP =** Nano-Sized Particles; **BAHAE** = *Borassus aethiopum* Hypocotyl Aqueous Extract; **TC** = Total Cholesterol; **TAG** = Triacylglycerol; **HDLC** = High Density Lipoprotein Cholesterol; **LDLC** = Low Density Lipoprotein Cholesterol.

The 200 mg/kg BW of BAHAE produced a serum LDH activity value that was well comparable ($p>0.05$) to that of fenofibrate (standard medication). Interestingly, while the 10 mg/kg BW of AgNP produced a serum cTnI value that compared well with the 20 mg/kg BW of AgNP, the 200 mg/kg BW of BAHAE also produced serum cTnI values that are comparable with those of the 400 mg/kg BW (Table 2). The induction of hyperlipidemia with Poloxamer-407, which substantially ($p<0.05$) lowered serum GPx, SOD, and CAT activities, increased serum MDA levels compared with DW-treated animals. In contrast, treatment of hyperlipidemic rats with all doses of AgNPs and BAHAE markedly ($p<0.05$) elevated serum activities of GP_x, SOD, and CAT, while lowering serum MDA levels compared with the DW-treated hyperlipidemic animals. In comparison, the 200 dose of BAHAE gave

© 2025 the authors. This work is licensed under the Creative Commons Attribution 4.0 International License

ISSN 2616-0684 (Print)
ISSN 2616-0692 (Electronic)

an MDA value that compared well with fenofibrate (p>0.05), and the 400 dose of the extract gave a GPx value that also compared well with fenofibrate (p>0.05). The 10 mg/kg BW of AgNP gave a serum MDA value that is comparable (p>0.05) with that of the 20 mg/kg BW of AgNP (Table 3).

Table 2: Effect of *Borassus aethiopum* hypocotyl aqueous extract and green silver nanoparticles on serum cardiac troponin I and some related enzyme markers in poloxamer-407 induced hyperlipidemic rats

Treatment Group	CK-MB (ng/mL)	cTnI (ng/mL)	LDH (U/L)
NR + DW	11.05±1.73[a]	6.24±1.74[a]	5.85±0.86[a]
HR + DW	52.75±1.82[b]	29.74±2.26[b]	26.46±3.24[b]
HR + Fenofibrate	27.49±1.72[c]	22.02±2.02[c]	18.38±2.06[c]
HR + 10 mg/kg body weight of NSP	18.72±2.36[d]	14.78±1.63[d]	15.24±1.72[d]
HR + 20 mg/kg body weight of NSP	22.82±2.28[e]	15.08±2.23[d]	10.86±1.68[e]
HR + 200 mg/kg body weight of BAHAE	35.87±3.62[f]	19.26±3.28[e]	17.26±1.91[c]
HR + 400 mg/kg body weight of BAHAE	31.92±3.76[g]	21.15±3.54[e]	20.72±2.57[f]

These results are the average ± SEM of five components. Superscripted results with values different from their respective sham control values down the column are not statistically significant (p<0.05)
NR = Normal Rats; **HR** = Hyperlipidemic Rats; **DW =** Distilled Water; **NSP =** Nano-Sized Particles; **BAHAE** = *Borassus aethiopum* Hypocotyl Aqueous Extract; **CK-MB** = Creatine Kinase (found in the heart muscle); **cTnI** = Cardiac Troponin I; **LDH** = Lactate Dehydrogenase

Table 3: Effect of *Borassus aethiopum* hypocotyl aqueous extract and green silver nanoparticles on serum enzymic and non-enzymic antioxidant markers in poloxamer-407 induced hyperlipidemic rats

Treatment Group	CAT (units/g tissue)	SOD (units/g tissue)	GP_x (units/g tissue)	MDA (units/g protein)
NR + DW	72.15±4.35[a]	61.28±4.24[a]	57.21±4.46[a]	2.65±0.03[a]
HR + DW	22.42±1.24[b]	17.85±1.45[b]	28.42±1.38[b]	15.26±1.45[b]
HR + Fenofibrate	31.07±2.75[c]	43.35±3.82[c]	41.64±3.26[c]	7.33±0.82[c]
HR + 10 mg/kg body weight of NSP	42.13±2.24[d]	38.64±2.67[d]	32.26±2.15[d]	5.38±0.27[d]
HR + 20 mg/kg body weight of NSP	48.78±2.56[e]	32.14±2.75[e]	38.04±3.64[e]	6.75±0.39[d]
HR + 200 mg/kg body weight of BAHAE	56.49±3.32[f]	48.67±3.34[f]	46.15±3.15[f]	8.24±0.98[c]
HR + 400 mg/kg body weight of BAHAE	61.25±3.47[g]	53.72±3.98[g]	42.92±3.82[c]	10.54±1.94[e]

Figures are average ± SEM of five determinants. Superscripted values having results different from their corresponding placebo values down the column are substantively different (p<0.05)
NR = Normal Rats; **HR** = Hyperlipidemic Rats; **DW =** Distilled Water; **NSP =** Nano-Sized Particles; **BAHAE** = *Borassus aethiopum* Hypocotyl Aqueous Extract; **CAT** = Catalase; **SOD** = Superoxide Dismutase; **GP_x** = Glutathione Peroxidase; **MDA =** Malondialdehyde.

The formation of silver nanoparticles was confirmed by a colour change from pale brown to deep brown (AgNPs), which occurred through the conversion of reduced silver ions (Ag^+) to silver (Ag) nanoparticles. The deep brown AgNPs were further confirmed by UV-Vis spectrophotometry, with their surface plasmon resonance properties: electrons in the AgNPs resonated and absorbed light, resulting in a plasmon band at 205 nm and an absorbance of 4.521. Furthermore, the AgNPs obtained from the BAHAE showed an absorbance peak between 200 and 300 nm, with the strongest resonance at 205 nm (Figure 1). FTIR analysis indicated bond types and peaks/functional groups involved in the synthesis and stabilization/capping of AgNPs in the 4000–650 cm-1 wavelength range. The AgNPs derived from BAHAE revealed prominent peaks mainly at wavelengths of 991.5, 1640.023 and 2922.23 cm^{-1}. Furthermore, the AgNPs synthesized from BAHAE

© 2025 the authors. This work is licensed under the Creative Commons Attribution 4.0 International License

ISSN 2616-0684 (Print)
ISSN 2616-0692 (Electronic)

which showed peaks at 991.5, 1640.023 and 2922.23 are characteristic of C-H, C–O, Ag–O/N (aromatics, ethers, metal-ligand bond/stretch); C=O (amide I), C=C, O–H bonding (proteins, water, alkenes) and C–H stretching (alkanes, surfactants, capping agents) respectively (Figure 2, Table 4). The diffraction angle represented the X-axis (2θ, degrees), while the extent of the diffracted X-rays quantified per second, and the quantity of crystalline substance contributing to each peak was represented by the Y-axis (Intensity, cps). The actual diffraction pattern of the AgNPs obtained from BAHAE is shown by the red line labeled 1_20250405_093728_G01_S01, while each peak corresponds to a set/group of crystallographic planes present in the AgNPs.

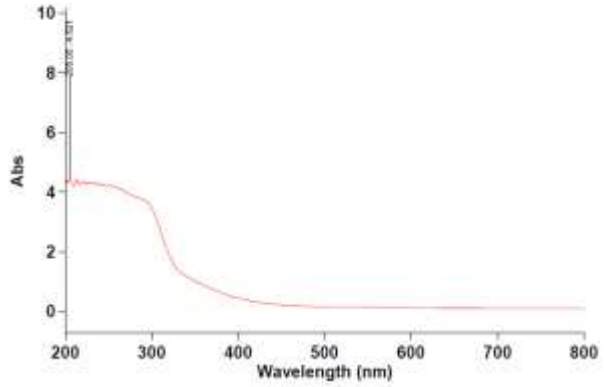

Figure 1: Ultraviolet-visible spectra of AgNPs synthesized from *Borassus aethiopum* hypocotyl aqueous extract

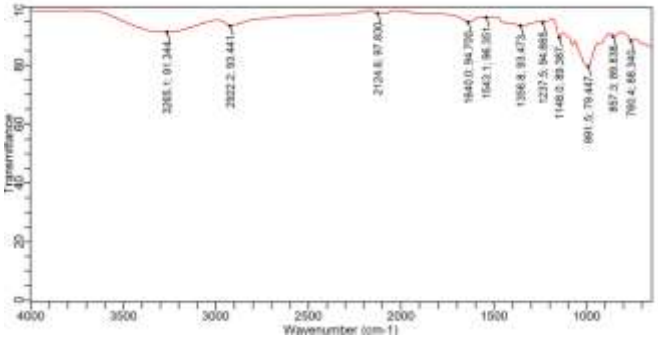

Figure 2: Fourier transform infrared (FTIR) spectra of silver nanoparticles obtained from *Borassus aethiopum* hypocotyl aqueous extract

Each peak/data obtained for the AgNPs was compared with well-known reference phases/materials, including silvialite, graphite, cristobalite, and urea, syn. The broad peak at low angle (10-30°) is typical of amorphous or nanocrystalline materials. The broad pattern/hump spanning ~10° to 30° indicates the silver nature of AgNPs and the presence of organic capping material or impurities such as urea. The sharp peaks observed between 30° and 70° correspond to various crystalline phases of the AgNPs. Furthermore, the XRD spectra and compressed image/pattern showed four prominent peaks at 2θ angles of 19.01°, 31.10°, 37.50°, and 46.20°, which correspond to the face cubic center (fcc) 89, 99, 111, and 230 planes of AgNPs, respectively (Figure 3a and b). At 20 µm, the surface morphology of the AgNPs from BAHAE showed a rough, irregular surface with many agglomerated particles. The material appears porous, as evidenced by the presence of voids or cavities between particles. Some particles have angular or faceted shapes, suggesting they may be crystalline or fractured. The particle also showed central features, including distinct polygonal or blocky particles (Figure 4a). The particle size ranges from ~1 µm to ~10 µm in diameter, with a heterogeneous particle size distribution (a combination of fine and coarse particles) (Figure 4c). The larger particles are embedded in a finer matrix (Figure 4a). At 50 µm, the surface morphology of the AgNPs from BAHAE showed a rough, irregular surface with agglomerated particles and cracks or voids running through it. The particle shape/size varied, with some roughly spherical and others angular, and bright spots (white areas) that may indicate denser materials, possibly silver-rich regions or contaminants (Figure 4b).

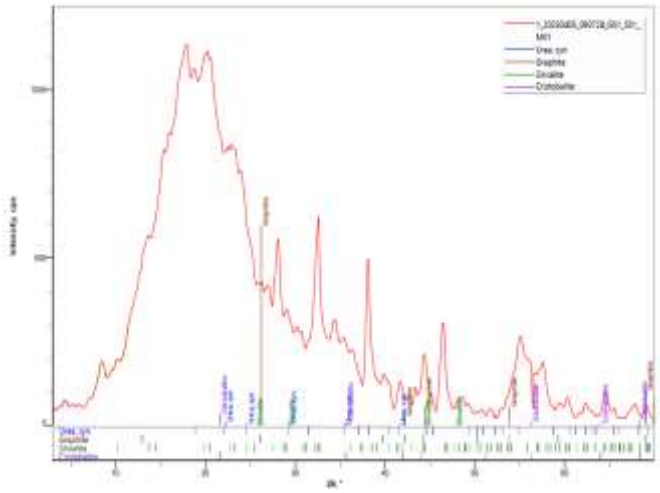

Figure 3a: XRD spectra of silver nanoparticles obtained from *Borassus aethiopum* hypocotyl aqueous extract

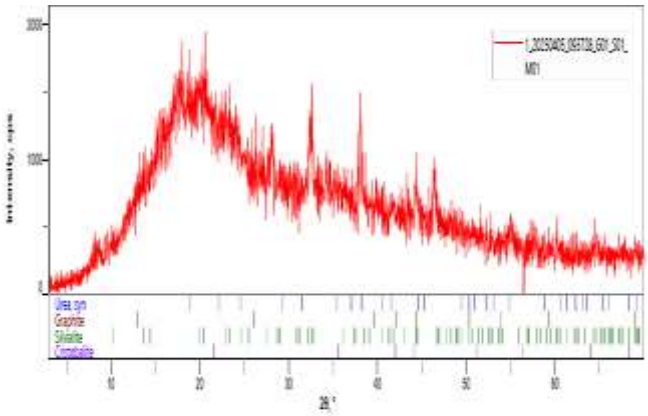

Figure 3b: XRD image of silver nanoparticles obtained from *Borassus aethiopum* hypocotyl aqueous extract

EDX analysis revealed that the BAHAE-AgNP area being imaged contained mostly carbon and other elements. Carbon had the highest content, with atomic (80.53) and weight (73.74) concentrations, respectively. This was followed by nitrogen, which had atomic and weight concentrations of 17.25 and 18.42, respectively. The least is calcium with atomic and weight concentrations of 0.03 and 0.10, respectively (Figure 4c and Table 5). The energy of the specific X-ray released by an element upon excitation by a major source of X-rays was represented by the X-axis (Energy in keV). In contrast, the number of X-ray photons observed at each energy level was represented on the Y-axis, with a very high peak indicating a high concentration of a particular element in the AgNP (Counts). In the EDXRF spectrum, the most prominent peaks between 22 keV and 25 keV are mainly the Ag Kα (~22.16 keV) and Kβ (~24.94 keV) lines. Small peaks for Fe (Iron) ~6.4 keV, Cu (Copper) ~8.0 keV, and Zn (Zinc) ~8.6–9.6 keV were also observed in the spectrum. Elements such as O (Oxygen) and possibly C (Carbon) were not well detected by the EDXRF device. The EDXEF spectrum did not show any prominent peaks for C, I, Na, or K (Figure 5, Table 6).

© 2025 the authors. This work is licensed under the Creative Commons Attribution 4.0 International License

ISSN 2616-0684 (Print)
ISSN 2616-0692 (Electronic)

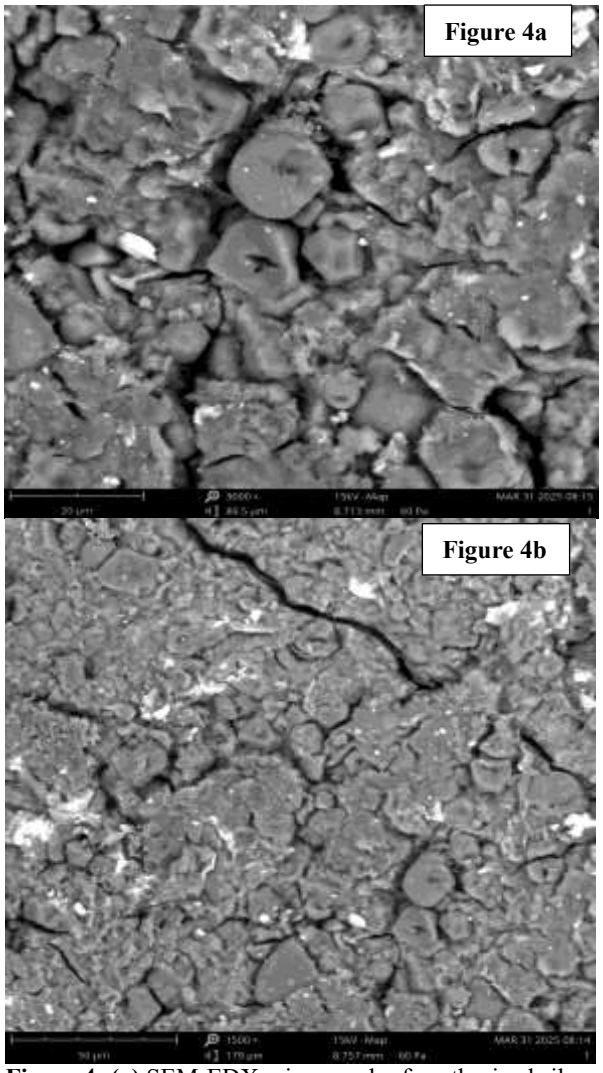

Figure 4: (a) SEM-EDX micrograph of synthesized silver nanoparticles obtained from *B. aethiopum* hypocotyl extract at 20 µm. **(b)** SEM-EDX micrograph of synthesized silver nanomaterials obtained from *B. aethiopum* hypocotyl extract at 50 µm.

The evaluation of green silver nanoparticles (AgNPs) derived from natural products in drug-induced hyperlipidemic animals can provide valuable insight into their potential lipid-lowering properties, which could help manage heart disease and related cardiac complications. LDLC is a type of lipoprotein particle that carries cholesterol and other fats through the bloodstream. It contributes to the accumulation of plaque in arteries, increasing the risk of heart disease and stroke.[33] The elevation in LDLC levels in the animals by poloxamer-407 could lead to the formation of plaque in the arteries (a condition called atherosclerosis). This plaque buildup narrows the arteries, restricting blood flow and potentially leading to heart attacks and strokes.[34-35] The reduction in LDLC concentration by the synthesized AgNPs and *Borassus aethiopum* hypocotyl aqueous extract (BAHAE) may be attributed to the ability of NSP and BAHAE to remove the buildup of plaques in the arteries. The plaque-free artery, mediated by AgNPs and BAHAE, would allow the free flow of blood through the arteries and prevent hyperlipidemia, heart disease, and related complications. Total cholesterol (TC) is a measure of the sum of all types of lipoprotein particles that carry cholesterol in the blood, which includes chylomicrons, LDLC, VLDLC, IDLC, HDLC, and TAG. It is a biomarker that indicates cardiovascular health status and helps assess the risk of heart disease and stroke.[36-38]

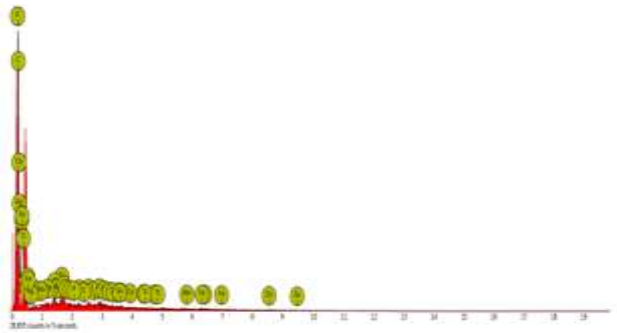

Figure 4c: Scanning Electron Microscopy with Energy Dispersive X-ray (SEM-EDX) Spectroscopy showing particle size distribution of synthesized silver nanoparticles obtained from *B. aethiopum* hypocotyl extract

The increase in TC in the animals following exposure to poloxamer-407 could lead to detrimental effects on heart health, evidenced by elevated levels of LDLC, VLDL, IDLC, and TAG, low HDLC, increased body weight, and thickening of the abdominal aorta wall.
These alterations lead to insulin resistance and inflammation, thereby facilitating the onset of atherosclerosis, a condition in which plaque accumulates in the arteries, causing heart problems.[39] The reduction in TC observed in this study may imply the cholesterol-lowering property of AgNPs and BAHAE, which it does by removing all types of bad lipoprotein (cholesterol) particles from the blood.

Table 4: Wavelength and intensity of FTIR analysis

Peak Number	Wavelength (cm^{-1})	Intensity
1	760.37692	88.33960
2	857.28770	89.83752
3	991.47186	79.44726
4	1148.02005	89.38735
5	1237.47616	94.66461
6	1356.75097	93.47337
7	1543.11786	96.35098
8	1640.02865	94.70021
9	2124.58257	97.82972
10	2922.23286	93.44053
11	3265.14795	91.34355

HDL cholesterol is a good cholesterol that plays a vital role in heart health and acts as a scavenger, transporting LDL cholesterol, a bad cholesterol, away from the arteries and back to the liver for removal from the biological system.[40] The low level of HDLC following induction with poloxamer-407 increases the risk of suffering from heart disease.[41] The high levels of HDL-cholesterol observed by administration of NSP, in this study, are protective for the heart since they help in the removal of cholesterol from the arteries. The high HDL-C levels induced by AgNPs could also promote cholesterol transport from peripheral tissues back to the liver for excretion, helping clear excess cholesterol from the body. TAGs are the main form of energy storage and a key component of adipose tissue. They are synthesized from glycerol and fatty acids and can be broken down (lipolysis) to release energy or stored for later use.[42,43] The low serum TAG level may imply accelerated stimulation for the breakdown of stored fats and the release of fatty acids for energy production by AgNPs.

© 2025 the authors. This work is licensed under the Creative Commons Attribution 4.0 International License

ISSN 2616-0684 (Print)
ISSN 2616-0692 (Electronic)

Table 5: Elemental composition of AgNPs synthesized from BAHAE by energy dispersive X-ray (EDX) spectroscopy

Element Number	Element Symbol	Element Name	Atomic Conc.	Weight Conc.
6	C	Carbon	80.53	73.74
7	N	Nitrogen	17.25	18.42
47	Ag	Silver	0.22	1.84
14	Si	Silicon	0.62	1.32
30	Zn	Zinc	0.24	1.20
13	Al	Aluminum	0.45	0.92
56	Ba	Barium	0.06	0.59
17	Cl	Chlorine	0.18	0.49
38	Sr	Strontium	0.07	0.44
25	Mn	Manganese	0.08	0.34
16	S	Sulfur	0.14	0.33
12	Mg	Magnesium	0.14	0.26
20	Ca	Calcium	0.03	0.10
11	Na	Sodium	0.00	0.00
19	K	Potassium	0.00	0.00
22	Ti	Titanium	0.00	0.00
26	Fe	Iron	0.00	0.00
15	P	Phosphorus	0.00	0.00
50	Sn	Tin	0.00	0.00

Conc. = Concentration

Creatine kinase MB (CK-MB), one of three isoenzymes of creatine kinase (CK), is an enzyme involved in energy production in muscle cells.[44,45] CK-MB is a cardiac biomarker mainly found in the heart muscle (myocardium) and helps diagnose and monitor cardiac health, especially in the early stage of heart damage and after heart reinfarction or reperfusion after treatment. When the heart muscle is damaged, CK-MB is released into the bloodstream at relatively high concentrations, making it a marker of heart muscle injury. Therefore, the reduced serum CK-MB level by NSP may be beneficial for the heart, as it suggests healthy heart muscle and the ability of NSP to restore the heart from damage caused by poloxamer-407 administration. Furthermore, the lowered CK-MB level induced by AgNPs in this study may not predispose the animals to heart attack, skeletal muscle injury, or other heart conditions, including myocarditis (inflammation of the heart muscle).

Cardiac troponin I (cTnI) is a protein complex, troponin, that controls muscle contraction in both skeletal and cardiac muscle.[46,47] In the heart, cTnI is found in the contractile proteins of muscle cells (myocytes). It is a specific biomarker for heart muscle damage, and elevated levels of CTnI in the blood indicate that the heart has been injured/damaged, primarily due to a heart attack. It is a key diagnostic marker for assessing heart health, particularly in cases of suspected myocardial infarction (heart attack). When heart muscle cells are damaged, cTnI is released into the bloodstream in high concentration. Therefore, the reduced serum cTnI level in this study indicates no heart cell damage and the ability of AgNPs to restore normal heart muscle function following poloxamer-407-induced damage in the animals. LDH is an enzyme that catalyzes the reversible conversion of lactate to pyruvate and plays a vital role in energy production and cellular respiration.[48,49] Elevated LDH levels in the blood can indicate tissue damage or cell death, making it a valuable marker for diagnosing and monitoring heart muscle disease. Damage to heart muscle cells, particularly during a heart attack (myocardial infarction), leads to the release of high LDH levels from the heart cells to the blood. Therefore, the reduced serum LDH activity in this study indicates that AgNPs can maintain heart homeostasis, thereby exerting beneficial cardiac protective effects.

Superoxide dismutase (SOD) is a family of enzymes that act as antioxidants, protecting the heart from oxidative stress.[50-52] SOD catalyzes the dismutation of superoxide radicals, a reactive oxygen species that can contribute to heart disease and heart failure, into hydrogen peroxide and molecular oxygen. The dismutation reaction catalyzed by SOD is essential because the superoxide radicals generated are highly reactive and can cause cellular damage if not neutralized. SOD therefore plays a significant role in improving cardiac function and reducing the risk of heart failure. The rise in serum SOD activity in this study may be attributed to AgNPs' antioxidant activity, which neutralizes the harmful superoxide radicals produced by poloxamer-407, thereby increasing serum SOD activity and protecting the animals' cardiac muscles against oxidative stress damage.

Catalase (CAT) is the enzyme that catalyzes the conversion of hydrogen peroxide (H_2O_2) to water and oxygen. The catabolism of H_2O_2 is crucial for protecting the heart muscle from oxidative damage caused by hydrogen peroxide, a byproduct of various cellular reactions.[53,54] CAT thus plays a protective antioxidant role in heart damage by reducing oxidative stress. Elevated CAT activity in the heart protects against heart failure and other cardiac dysfunctions, especially those associated with oxidative stress and adverse remodeling. The increased serum SOD activity in this study may be attributed to AgNPs' ability to protect heart cells from oxidative damage induced by H_2O_2 generated by poloxamer-407, leading to the observed rise in CAT activity.

Malondialdehyde (MDA) is a biomarker of lipid peroxidation and oxidative stress, and elevated levels indicate severe heart damage.[55,56] MDA indicates oxidative stress status and contributes to the onset and progression of cardiovascular disorders, including coronary heart disease and heart failure. In atherosclerosis, in addition to harmful cholesterol, oxidative stress contributes to the formation of plaque in the coronary arteries, which can restrict blood flow to the heart and lead to heart attacks. In heart failure, oxidative stress can damage heart muscle cells, impairing their ability to contract and pump blood effectively. The reduced serum MDA level in this study may be attributed to AgNPs' ability to reduce plaque formation in the coronary artery. This will allow the free flow of blood to and from the heart, thereby reducing the risk of a heart attack. Glutathione peroxidase (GPx) is an antioxidant enzyme that plays an essential role in protecting the heart against oxidative stress-induced damage.[57,58] It helps neutralize harmful reactive oxygen species (ROS), such as H_2O_2, preventing heart damage and dysfunction. The increased serum GPx activity in this study could be attributed to AgNPs' antioxidant activity, which neutralizes the harmful effects of H_2O_2 produced by poloxamer-407, thereby protecting the animals' hearts.

UV-Visible spectroscopy is an analytical procedure that measures the quantity of visible or ultraviolet light absorbed or transmitted by a material. This method works on the principle that substances absorb specific wavelengths of light, and the extent of absorption is proportional to the concentration of the substance. The spectroscopic technique is primarily used to characterize molecules by identifying compounds and quantifying their presence.[59-61] In the present study, UV-Vis spectroscopy played an essential role in confirming the synthesis of AgNPs from BAHAE by a characteristic surface plasmon resonance (SPR) band between 200–300 nm. The ability of BAHAE to participate in the synthesis of AgNPs is attributed to its phytoconstituents, such as flavonoids and phenolics, which possess inherent reducing properties. The UV-Vis findings confirm this, with a unique SPR peak at 205nm indicating active bioreduction.

© 2025 the authors. This work is licensed under the Creative Commons Attribution 4.0 International License

ISSN 2616-0684 (Print)
ISSN 2616-0692 (Electronic)

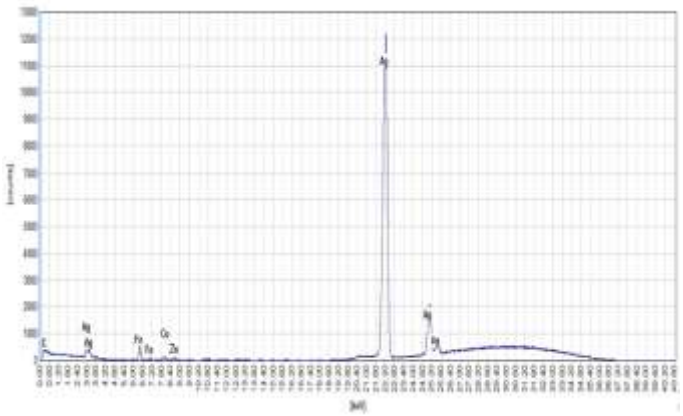

Figure 5: Energy dispersive X-ray fluorescence (EDXRF) chromatogram of silver nanoparticles synthesized from *Borassus aethiopum* hypocotyl aqueous extract

This is because, biosynthesized nanoparticles containing phytochemicals with reducing (antioxidant) properties can lower hyperlipidemia in experimental models. When encapsulated in nanoparticles, phytochemicals can be delivered more effectively to target cells and tissues, potentially reducing elevated lipid levels in the biological system. Furthermore, the UV-Vis spectra revealed the reduction of silver ions in the silver-complexed solution during the reaction with components inherent to BAHAE. This was evidenced by the upregulation and excitation of Plasmon vibrations of AgNPs in solution, which signify the reduction of silver ions to AgNPs. FTIR spectroscopy is a technique that helps identify the chemical composition and structure of a substance. It also provides insight into the identification of the functional groups and bond types involved in the biosynthesis and stabilization of AgNPs.[62] In this study, the FTIR results indicated absorption peaks that identified functional groups, namely phytochemicals, in the AgNPs, which act as reducing, capping, and antihyperlipidemic agents. The prominent peaks observed for the synthesized AgNP at 991.5 cm^{-1}, 1640.023 $cm^{-1,}$ and 2922.23 cm^{-1} could be attributed to typical vibrational patterns of molecular bonds or functional groups that might be available in the AgNPs derived from BAHAE for capping/stabilization or for interaction with the biological system for downregulation of the cholesterol biosynthetic pathway for controlling hyperlipidemia. SEM provides details of the surface morphology and structure, while EDX gives insight into the elemental composition of a substance. SEM spectroscopy is also used to analyze pore and fiber metrics, to characterize surface topography of specimens, and to determine particle size for nanosized materials.[63,64] The cracks observed in the SEM spectra of AgNPs obtained from BAHAE may be caused by drying shrinkage, sample preparation stress, or thermal contraction, rather than intrinsic material failure. The bright spots (white areas) may indicate denser materials-possibly silver-rich regions or contaminants. The presence of particles with angular or faceted shapes suggests that they might be crystalline or fractured. The larger particles embedded in a finer matrix may have resulted from incomplete mixing, sintering, or agglomeration. The porosity and irregular particle shapes observed may indicate incomplete sintering, dehydration of hydrated phases, or the presence of unreacted precursors. Furthermore, energy-dispersive X-ray (EDX) spectroscopy values obtained during SEM, namely atomic and weight concentrations, indicate the number of silver ions relative to all atoms on the particle's surface and the mass proportion of silver relative to the total weight of the elements observed. The high EDX value of the AgNPs obtained for the element carbon (atomic concentration of 80.53% and a weight concentration of 73.74%) both indicates its high silver content as well as high pure status of the AgNP system, suggesting that the antihyperlipidemic activity observed in this study could be, in part, attributed to silver. Owing to the documented antioxidant and hypolipidemic effects of AgNPs, such a high silver concentration may enhance their biological activity by modulating lipid metabolism pathways.[65] This could contribute to the observed antihyperlipidemic effect, potentially through mechanisms such as reduction of oxidative stress (inhibition of lipid peroxidation) and modulation of the lipid biosynthetic key regulatory enzymes.

Table 6: Elemental composition of AgNPs synthesized from BAHAE by EDXRF

Element	Concentration	Peak (cps/mA)	Background(cps/mA)
Fe	0.06145%	1040	13
Cu	0.000995%	54	19
Ni	0.00794%	14	6
Zn	0.00436%	199	10
Al	0.02061%	427	1151
Mg	0.00592%	37	188
Na	[0.0032] %	1	74
S	0.08615%	1240	812
P	0.04011%	387	487
Ca	0.04438%	242	38
K	0.01629%	88	330
Mn	0.002498%	136	171
Rb	0.000235%	1	4
Sr	0.000342%	2	3
Br	0.00085%	2	3
Cl	0.1904%	333	-38
Cr	0.000164%	8	76
V	0%	11	36
W	0.0509%	31	-9
Bi	0.311%	3	5
Sn	0%	0	145
Si	[0.14] %	0	31
As	0%	0	7
Nb	[0.0052] %	1	2
Ta	0.1404%	20	37
Ag	0.2757%	669	1218
Pb	0.333%	4	4

X-ray diffraction (XRD) is an analytical technique used to characterize the crystallographic structure (texture), phases, and atomic arrangement in crystalline materials. It provides insight into the composition of a material, phase identification, and other structure-based lattice parameters, such as crystallinity, strain, average particle weight, and crystal deformities. The peaks of XRD are formed by the ordered interaction of a single X-ray image distributed at specific locations

© 2025 the authors. This work is licensed under the Creative Commons Attribution 4.0 International License

away from each group of lattice levels in a particle. The peak intensities are determined by the even distribution of atoms within the grid.[66,67] In the study, the broad bending pattern and the absence of clear-cut silver peaks may indicate the presence of amorphous and ultra-fine AgNPs in BAHAE. Nanosized particles with these features exhibit a large surface area and robust interactions with biomembranes, enabling bioactivity and the easy delivery of medications. This feature is crucial for drug-delivery silver agents, thereby facilitating lipid-lowering effects via targeted oxidative modulation and improved drug bioavailability, as evidenced in the *in vivo* study. AgNPs possess antioxidative properties that are vital for the management of hyperlipidemia. The amorphous structural pattern observed by XRD of the AgNPs in this study supports the formation of a stable nanocomposite capable of interacting with the cholesterol metabolic pathway. The combined interaction of the nanostructured system with Ag's bioactivity might inhibit lipid peroxidation, improve lipid profile, and modulate relevant cardiac biomarkers, including VLDLC, CTnI, cholesterol, CK-MB, and TAG. The most conspicuous peaks at 22.16 keV and ~24.94 keV for Ag confirm that silver is the dominant constituent, as is typical of most AgNPs. The small peaks of Ag observed at 2.98 keV and 6.60 keV indicate L-series emission. The presence of these small elements may also indicate residues from synthesis, impurities, components of the capping/stabilizing agents, or substrate or background material. The lack of a significant peak for K, Cl, and Na may be attributed to minimal contamination of the AgNPs by common salts. In the present study, the presence of these trace elements was minimal, suggesting that the nanoparticles are composed mainly of elemental silver, indicative of a high degree of purity.

Energy-dispersive X-ray fluorescence (EDXRF) is a non-destructive analytical technique that analyzes and identifies the elements present in a material. It operates by detecting the characteristic X-rays emitted by a sample upon exposure to X-rays, thereby providing information about the elements present in the substance.[68,69] The EDXRF analysis of the AgNPs derived from BAHAE revealed a few trace elements, including Cr, Mn, Fe, Ni, Zn, V, Ag, As, Pb, Cu, out of the 27 elements identified. The presence of these trace elements, which are minimal within the biological system, suggests that the AgNPs are composed mainly of elemental silver, indicating a high degree of purity. The high purity of AgNPs reduces toxicological interactions and enhances their desired bioactivity. The absence of significant contamination in the EDXRF profile further supports the biosafety of the AgNPs, which is critical when considering long-term therapeutic use. Therefore, the EDXRF analysis did not only confirm the synthesis of AgNPs but also supports their suitability for biomedical applications, including their probable role in managing hyperlipidemia via modulation of oxidative stress pathways, improving antioxidant enzyme activity, and reducing inflammatory responses, impact on lipid metabolism by their interaction with hepatic cells, potential enhancement of lipid clearance or modulating gene expression related to lipid synthesis and breakdown, all of which are crucial indicators in the management of hyperlipidemia.[70-72]

Conclusion

Green AgNPs obtained from BAHAE normalized the poloxamer-407-induced hyperlipidemic alterations in the animals by increasing antioxidant levels and reducing elevated serum lipid levels, oxidative stress, and cardiac biomarkers, compared with the aqueous extract. The characterization of the synthesized AgNPs not only provides information about the morphology/crystalline structure/functional group/elemental composition of AgNPs but also plays a significant role in understanding the interaction of the particles inherent in AgNPs with the biological system for managing hyperlipidemia via their bioavailability, modulation of the oxidative stress pathways, and downregulation of the cholesterol metabolic pathway. Therefore, the AgNPs obtained from *Borassus aethiopum* hypocotyl could be explored in the management of hyperlipidemia.

Conflict of Interest

The authors declare no conflict of interest.

Authors' Declaration

The authors hereby affirm that the findings contained in this article are original and that any liability for claims relating to the content of this article will be borne by them.

Acknowledgements

The authors truly recognize and thank the laboratory support team in the Biochemistry Department, Baze University, Abuja, for their technical assistance during plant extraction. We also appreciate the assistance of Mr. Lateef A. Akeem of the Herbarium and Ethnobotany Unit, NIPRD, Idu, Abuja for his work in getting the Voucher Specimen Number of the plant.

References

1. Visseren FLJ, Mach F, Smulders YM. ESC guidelines on cardiovascular disease prevention in clinical practice. Eur Heart J. 2021; 42 (34): 3227–3237. https://doi.org/10.1093/eurheartj/ehab484.
2. Pirillo A, Norata GD. The burden of hypercholesterolemia and ischemic heart disease in an ageing world. Pharmacol Res. 2023; 193: 106814. https://doi.org/10.1016/j.phrs.2023.106814.
3. Pirillo A, Casula M, Olmastroni E, Norata GD, Catapano AL. Global epidemiology of dyslipidaemias. Nat Rev Cardiol. 2021; 18 (10): 689-700. doi: 10.1038/s41569-021- 00541 4.
4. WHO (World Health Organization), Global health observatory data repository, Geneva: World Health Organization; Available: https://apps.who.int/gho/data/view.main.2467?lang=e n. 2016.
5. Savarese G, Becher PM, Lund LH, Seferovic P, Rosano GMC, Coats AJS. Global burden of heart failure: a comprehensive and updated review of epidemiology. Cardiovasc Res. 2022; 118: 3272–3287.
6. Pirillo A, Tokgozoglu L, Catapano AL. European Lipid Guidelines and Cardiovascular Risk Estimation: Current Status and Future Challenges. Curr Atheroscler Rep. 2024; 26 (5): 133-137. doi: 10.1007/s11883-024-01194-7.
7. Oh RC, Trivette ET, Westerfield KL. Management of Hypertriglyceridemia: Common Questions and Answers. Am Family Phys. 2020; 102 (6): 347–354.
8. Thomson MJ, Serper M, Khungar V, Weiss LM, Trinh H, Firpi-Morell R, Roden M, Loomba R, Barritt AS, Gazis D, Mospan AR, Fried MW, Reddy KR, Lok AS. Prevalence and Factors Associated with Statin Use Among Patients with Nonalcoholic Fatty Liver Disease in the TARGET-NASH Study. Clin Gastroenterol Hepatol. 2022; 20 (2): 458-460.e4.
9. Sizar O, Khare S, Patel P, Talati R. Statin Medications. [Updated 2024 Feb 29]. In: StatPearls [Internet]. Treasure Island (FL): StatPearls Publishing. Available from: https://www.ncbi.nlm.nih.gov/books/NBK430940/. 2024.
10. Egwu CO, Aloke C, Onwe KT, Umoke CI, Nwafor J, Eyo RA, Chukwu JA, Ufebe GO, Ladokun J, Audu DT, Agwu AO, Obasi DC, Okoro CO. Nanomaterials in Drug Delivery: Strengths and Opportunities in Medicine. Molecules. 2024; 29 (11): 2584. doi: 10.3390/molecules29112584.
11. Picraux ST. Nanotechnology. *Encyclopedia Britannica*, https://www.britannica.com/technology/nanotechnology. Accessed May 24, 2025.
12. Bayda S, Adeel M, Tuccinardi T, Cordani M, Rizzolio F. The History of Nanoscience and Nanotechnology: From Chemical-Physical Applications to Nanomedicine. Molecules. 2019; (25) (1): 72-112. doi: 10.3390/molecules25010112.
13. Vincent A, Esumaba SA, Jacob K, Nadratu MB, Fidelis MK. Development and Evaluation of African Palmyra Palm (*Borassus aethiopum*) Fruit Flour-Wheat Composite Flour Noodles. Congent Food Agric. 2020; 6 (1): 174-176.
14. Salako KV, Moreira F, Gbedomon RC, Tovissode F, Assogbadjo AE, Kakai RLG. Traditional Knowledge and Cultural

© 2025 the authors. This work is licensed under the Creative Commons Attribution 4.0 International License

Importance of *Borassus aethiopum* Mart. In Benin: Interacting Effects of Socio-Demographic Attributes and Multi-Scale Abundance. J Ethnobiol Ethnomed. 2018; 14(1): 36-46.
15. Aduwamai UH, Mahmud BA, Daniel D. Antioxidant and Antihyperlipidemic Activity of Methanol Extract of *Borassus aethiopum* Fruit in Triton X-100 Induced Hyperlipidemic Rats. Am J Biochem. 2019; 9 (2): 35-44. doi: 10.5923/j.ajb.20190902.03.
16. Maniru N, Onuigwe FU, Wali U, Oluranti AC, Abdulrahman Y, Buhari HA, Kwaifa IK, Ibrahim AB. Effect of Methanolic Fruit Extract of *Borassus aethiopum* on Body Mass Index and Lipid Profile Parameters of High-Fat Diet-Induced Obese Wistar Rats. Bayero J Med Lab. Sci. 2024; 9 (1): 136–144.
17. Adams MD, Eze ED. *Borassus aethiopum* (Mart..) ethanol fruit extract reverses alloxan-treatment alterations in experimental animals, Mediterr. J Nutr Metab. 2022; 15 (3): 429-445. DOI:10.3233/MNM-211589
18. Naseem K, Zia-Ur-Rehman M, Ahmad A, Dubal D, Al-Garni TS. Plant Extract-Induced Biogenic Preparation of Silver Nanoparticles and Their Potential as Catalyst for the Degradation of Toxic Dyes. Coatings. 2020; 10(12):1235. https://doi.org/10.3390/coatings10121235
19. Li H, Dutkiewicz EP, Huang YC, Zhou HB, Hsu CC. Analytical methods for cholesterol quantification. J Food Drug Anal. 2019; 27 (2): 375-386. https://doi.org/10.1016/j.jfda.2018.09.001.
20. Warnick GR, Wood PD. National Cholesterol Education Program Recommendations for Measurement of High-Density Lipoprotein Cholesterol: Executive Summary, Clin Chem. 1995; 41 (10): 1427-1433.
21. Islam SMT, Osa-Andrews B, Jones PM, Muthukumar AR, Hashim I, Cao J. Methods of Low-Density Lipoprotein-Cholesterol Measurement: Analytical and Clinical Applications. EJIFCC. 2022; 33(4): 282-294.
22. Fossati P, Prencipe L. Serum triglycerides determined colorimetrically with an enzyme that produces hydrogen peroxide. Clin Chem. 1982; 28 (10): 2077–2080. https://doi.org/10.1093/clinchem/28.10.2077.
23. Ben-Attig J, Latrous L, Galvan I, Zougagh M, Rios A. Rapid determination of malondialdehyde in serum samples using a porphyrin-functionalized magnetic graphene oxide electrochemical sensor. Anal Bioanal Chem. 2023; 415 (11): 2071-2080. Doi: 10.1007/s00216-023-04594-x.
24. Krishna H, Avinash K, Shivakumar A, Al-Tayar NGS, Shrestha AK. A quantitative method for the detection and validation of catalase activity at physiological concentrations in human serum, plasma, and erythrocytes. (Spectrochimica Acta Part A). Mol Biomol Spectrosc. 2021; 251: 119358. https://doi.org/10.1016/j.saa.2020.119358.
25. Sun Y, Oberley L, Li Y. A simple method for clinical assay of superoxide dismutase. Clin Chem. 1988; 34: 497–500. doi: 10.1093/clinchem/34.3.497.
26. Nwakulite A, Obeagu EI, Eze R, Ugochi VE, Vincent C, Okafor CJ, Chukwurah EF, Unaeze BC, Amaechi CO, Okwuanaso CB, Chukwuani U, Ifionu BI. Estimation of Serum Glutathione Peroxidase in Streptozotocin-Induced Diabetic Rat Treated with Bitter Leaf Extract. J Pharm Res Int'l. 2021; 33 (30B): 200–206. doi: 10.9734/jpri/2021/v33i30B31655.
27. Babuin L, Jaffe AS. Troponin: the biomarker of choice for the detection of cardiac injury. Can. Med Assoc J. 2005; 173 (10): 1191-1202. DOI: 10.1503/cmaj/051291.
28. Tate JR, Bunk DM, Christenson RH, Katrukha A, Noble JE, Porter RA, Schimmel H, Wang L, Panteghini M. Standardization of cardiac troponin I measurement: past and present. Pathol. 2010; 42 (5): 402-408. https://doi.org/10.3109/00313025.2010.495246.
29. Gerhardt W, Ljungdahl L, Borjesson J, Hofvendahl S, Hedenas B. Creatine kinase B-B-subunit activity in human serum. I. Development of an immunoinhibition method for routine determination of S-creatine kinase B-subunit activity. Clinica Chimica Acta. 1977; 78 (1): 29-41. https://doi.org/10.1016/0009-8981(77)90335-7.
30. Rchid SM, El-Azzouzi MK, Krimi K, El-Moujtahide D, Sebbar E, Choukri M.Verification of analytical performance of Creatine Kinase isoenzyme MB (CK-MB) on the Alinity c® Experience from the Biochemistry Laboratory of Mohammed VI University Hospital in Oujda. GSC Biol Pharm Sci. 2025; 30 (01): 201-205. DOI: https://doi.org/10.30574/gscbps.2025.30.1.0026.
31. Glowacka J, Wisniewska A, Koncki R, Strzelak K. Photometric flow system for the determination of serum lactate dehydrogenase activity. Talanta. 2023; 265: 124817.
32. Sari D, Endardjo S, Irawati D. Blood lactate level in Wistar rats after four-and-twelve week intermittent aerobic training. Med J Indones. 2013; 22: 141-149. DOI: 10.13181/mji.v22i3.582].
33. Mallikarjuna RB, Vedavijaya T, Ramani YR, Sayana SB. Protective Role of Methanol Leaf Extract of *Catharanthus Roseus* in Lipid Profile Modulation in Diabetic Wistar Rats. Cureus. 2025; 14:17 (1): e77420. Doi: 10.7759/cureus.77420.
34. Atsukwei D, Eze ED, Adams MD, Seriki SA, Ukpabi CN. Hypolipidaemic Effect of Ethanol Leaf Extract of *Moringa Oleifera* Lam. in Experimentally induced Hypercholesterolemic Wistar Rats. Int'l J Nutr Food Sci. 2014; 3 (4): 355-360. doi: 10.11648/j.ijnfs.20140304.28.
35. Ayo VI, Adondua MA, Morayo AE, Ekele J, Amilo D, Ochuele DA, Ayantse LM, Barrah C, Abdulsalam IO, Eya SB, Iheanacho CC, Tibile ST, Mohammed RI, Barde CE. Effect of *Lactuca sativa* supplemented diet on Poloxamer-407-induced hyperlipidemic albino rats (*Rattus norvegicus*). Asian J Nat Prod Biochem. 2023; 21 (2): 67-78. DOI: 10.13057/biofar/f210203.
36. Adams MD, Sharubutu BG, Olaolu TD. Molecular docking, HPLC phytochemical profiling and androgenic property of ethylacetate fraction of B*orassus aethiopum* (Mart.) hypocotyl in pre-clinical models. J Ethnopharmacol. 2026; 354: 120494. https://doi.org/10.1016/j.jep.2025.120494.
37. Adams MD, Manu HA, Enyioma-Alozie S. Molecular Docking, Contraceptive Property and Histopathological Changes in Experimental Models by *Digitaria exilis* Grain Extract via Interference with Steroidogenesis at Ovarian Level. Trop J Nat Prod Res. 2025; 9(7): 3349–3359. https://doi.org/10.26538/tjnpr/v9i7.6
38. Dzhelebov SP, Trifonova K. Poloxamer 407-induced chronic hyperlipidemia is not associated with disorders of blood glucose level. Trakia J Sci. 2025; 23 (1): 22-29. doi:10.15547/tjs.2025.01.002.
39. Pham VAT, Pham PX, Tran TT, Dang HTT, Trinh QV, Dau DT. Effect of a nature-derived combination of *Ananas comosus* and *Bambusa bambos* (L.) in hyperlipidemic experimental animals. Trop J Nat Prod Res. 2025; 9 (5): 2323–2328. https://doi.org/10.26538/tjnpr/v9i5.61.
40. Bawa I, Uti DE, Itodo MO, Umoru GU, Zakari S, Obeten UN. Effect of Solvent Extracts of *Tephrosia vogelii* Leaves and Stem on Lipid Profile of Poloxamer 407-Induced Hyperlipidemic Rats. Ibnosina J Med Biomed Sci. 2022; 14: 135–144. https://doi.org/ 10.1055/s-0042-1760223.
41. Naik HG, Kolur A, Maled D, Khanwelkar CC, Desai R, Gidamudi S. Effect of Poloxamer-407 on VLDL, LDL, and HDL. Nat J Physiol Pharm Pharmacol. 2014; 4 (3): 221–224. DOI: 10.5455/njppp.2014.4.040620141
42. Kelle BP, Cesic AK, Custovic S, Cosovic E, Lagumdzija D, Jordamovic N, Kusturica J. Improvement of a diet-induced model of hyperlipidemia in Wistar rats: Assessment of biochemical parameters, the thickness of the abdominal aorta, and liver histology. J King Saud Univ – Sci. 2024; 36 (2): 103068. https://doi.org/10.1016/j.jksus.2023.103068.

© 2025 the authors. This work is licensed under the Creative Commons Attribution 4.0 International License

43. Okere OS, Adams MD, Orji CG. Chemical Composition, *In vivo* Immunomodulatory and Anti-Hyperlipidaemic Properties of R*hinoceros* (*Rhino*) Oil in Lead-Induced Immunocompromised Models. J Phytomed Therapeut. 2022; 21 (2): 931–974. *https*://dx.doi.org/10.4314/jopat.v21i2.15.
44. Nair SM, Pareek A, Jamali MC. Assessment of Biochemical Markers for Early Detection and Monitoring of Cardiovascular Diseases: Myocardial Infarction and Heart Failure. Qual Assur. 2024; 15 (1): 288-295. https://doi.org/10.25258/ijpqa.15.1.43.
45. Wu J, Qin M, Gao Y, Liu Y, Liu X, Jiang Y, Yang Y, Gao Y. Association between fluoride exposure and the risk of serum CK and CK-MB elevation in adults: a cross- sectional study in China. Front. Public Health. 2025; 12: 1410056. doi: 10.3389/fpubh.2024.1410056.
46. Herman E, Knapton A, Rosen E, Zhang J, Estis J, Agee SJ, Lu QA, Todd JA, Lipshultz SE. Baseline serum cardiac troponin I concentrations in Sprague-Dawley, spontaneous hypertensive, Wistar, Wistar-Kyoto, and Fisher rats as determined with an ultrasensitive immunoassay, Toxicol Pathol. 2011; 39 (4): 653-663. doi: 10.1177/0192623311406931.
47. Reuben E, Chinko BC, Batubo NP, Amah-Tariah FS. Impact of Intermittent Fasting on Serum Cardiac Biomarkers in Male Wistar Rats. Int'l J Clin Exp Med Sci. 2025; 11(1): 11-17. https://doi.org/10.11648/j.ijcems.20251101.12.
48. Rahman MF, Siddiqui, MK, Jamil K. LDH profiles of male and female rats treated with Vepacide. Phytother Res. 2002; 16(2): 122-126. doi: 10.1002/ptr.809.
49. Guo P, Ding H, Li X, Xie D, Wang K, Su W, Yang X, Nie F, Wang P. Association between lactate dehydrogenase levels and all-cause mortality in ICU patients with heart failure: a retrospective analysis of the MIMIC-IV database, BMC Cardiovasc Disord. 2025; 25 (62): 121- 129. https://doi.org/10.1186/s12872-025-04513-1.
50. van Deel ED, Lu Z, Xu X, Zhu G, Hu XT, Oury D, Bache RJ, Duncker DJ, Chen Y. Extracellular superoxide dismutase protects the heart against oxidative stress and hypertrophy after myocardial infarction. Free Radic Biol Med. 2008; 1:44 (7): 1305-1313. Doi: 10.1016/j.freeradbiomed.2007.12.007.
51. Cairns M, Odendaal C, O'Brien C, Marais E, Oestlund I, Storbeck K, Sishi B, Joseph D, Smith C, Essop MF. Effects of chronic stress on rat heart function following regional ischemia: a sex-dependent investigation. Am J Physiol-Heart Circulat Physiol. 2024; 327 (4): H880-H895. https://doi.org/10.1152/ajpheart.00424.2024.
52. Zhao B, Peng J, Chen C, Fan Y, Zhang K, Zhang Y, Huang X. Innovative engineering of superoxide dismutase for enhanced cardioprotective biocatalysis in myocardial ischemia-reperfusion injury. Int'l J Biol Macromol. 2025; 286: 137656. https://doi.org/10.1016/j.ijbiomac.2024.137656.
53. Qin F, Lennon-Edwards S, Lancel S, Biolo A, Siwik DA, Pimentel DR, Dorn GW, Kang YJ, Colucci WS. Cardiac-specific overexpression of catalase identifies hydrogen peroxide-dependent and -independent phases of myocardial remodeling and prevents the progression to overt heart failure in G(alpha)q-overexpressing transgenic mice. Circ Heart Fail. 2010; 3 (2): 306-313. Doi: 10.1161/CIRCHEARTFAILURE.109.864785.
54. Pendergrass KD, Varghese ST, Maiellaro-Rafferty K, Brown ME, Taylor WR. Davis ME, Temporal Effects of Catalase Overexpression on Healing After Myocardial Infarction, Circ: Heart Fail. 2011; 4 (1): 98-106. https://doi.org/10.1161/CIRCHEARTFAILURE.110.957712.
55. Lankin VZ, Tikhaze AK, Melkumyants AM. Malondialdehyde as an Important Key Factor of Molecular Mechanisms of Vascular Wall Damage under Heart Disease Development. Int'l J Mol Sci. 2023; 24 (1): 128. https://doi.org/10.3390/ijms24010128.
56. Hadi AN, Zaidi IA, Kamal Z, Ashraf AD, Khan RU, Rumman GT, Khan MH, Omair F. Estimation of Serum Malondialdehyde (a Marker of Oxidative Stress) as a Predictive Biomarker for the Severity of Coronary Artery Disease (CAD) and Cardiovascular Outcomes, Cureus. 2024; 16 (9): e69756. DOI 10.7759/cureus.69756.
57. Ojetola AA, Adedeji TG, Fasanmade AA. Changes in antioxidant status, atherogenic index, and cardiovascular variables after prolonged doses of D-ribose-L-cysteine in male Wistar rats. Heliyon. 2021; 7 (2): e06287. https://doi.org/10.1016/j.heliyon.2021.e06287.
58. Eze ED, Afodun AM, Sulaiman SO, Ponsiano N, Iliya E, Adams MD, Okpanachi AO, Rabiu KM. Lycopene attenuates diabetes-induced oxidative stress in Wistar rats. J Diab Endocrinol. 2018; 9 (2): 11-19. DOI: 10.5897/JDE2018.0118.
59. Abdel-Hafeez AM, Abdel-Goad MA. Silver Nanoparticles from Nature: Green Synthesis Methods and Applications - A Review. J Adv Engr Trend. 2025; 41 (4): 227-236.
60. Toufique A, Tugrul RO, Gulnaz O. Multifarious Uses of UV-VIS Spectroscopy for Green Synthesis of Silver Nanoparticles for Antibacterial Textiles. Textil Leath Rev. 2024; 7: 176-202. https://doi.org/10.31881/TLR.2024.014.
61. Villagran Z, Anaya-Esparza LM, Velazquez-Carriles CA, Silva-Jara JM, Ruvalcaba-Gomez JM, Aurora-Vigo EF. Rodriguez-Lafitte E, Rodriguez-Barajas N, Balderas-Leon I, Martinez-Esquivias F, Plant-Based Extracts as Reducing, Capping, and Stabilizing Agents for the Green Synthesis of Inorganic Nanoparticles. Resour. 2024; 13 (6): 70. https://doi.org/10.3390/resources13060070.
62. Pasieczna-Patkowska S, Cichy M, Flieger J. Application of Fourier Transform Infrared (FTIR) Spectroscopy in Characterization of Green Synthesized Nanoparticles. Molecules. 2025; 30 (3): 684. https://doi.org/10.3390/molecules30030684.
63. Lekkala VD, Muktinutalapati VVAV, Lebaka VR, Lomada D, Korivi M, Li W, Reddy MC. Green Synthesis and Characterization of Silver Nanoparticles from *Tinospora cordifolia* Leaf Extract: Evaluation of Their Antioxidant, Anti-Inflammatory, Antibacterial, and Antibiofilm Efficacies. Nanomaterials. 2025; 15 (5): 381-389. https://doi.org/10.3390/nano15050381.
64. Kakol M, Tagliasacchi E, Borkowski A, Slowakiewicz M. Influence of different sample preparation techniques on imaging viruses and virus-like particles by scanning electroand scanning transmission electron microscopes. Front. Microbiol. 2023; 14: 1279720. doi: 10.3389/fmicb.2023.12797
65. Irshad M, Shah L, Shujaat N, Khan M, Niaz Z, Ullah I. Green Synthesis and Characterization of Silver Nanoparticles Using *Lespedeza juncea* Extract: An Insight Into Its Antibacterial, Antifungal, and Enzyme Inhibitory Potential. Microsc Res Tech. 2025; 16: 1-15. doi: 10.22541/au.172892530.01193795/v1.
66. El-Baz YG, Moustafa A, Ali MA, El-Desoky GE, Wabaidur SM, Iqbal A. Green synthesized silver nanoparticles for the treatment of diabetes and the related complications of hyperlipidemia and oxidative stress in diabetic rats. Exp Biol Med. 2024; 248 (23): 2237-2248. doi:10.1177/15353702231214258
67. Saba M, Farooq S, Alessa AH, Bektas KI, Belduz AO, Khan AZ, Shah AA, Badshah M, Khan S. Green synthesis of silver nanoparticles using Keratinase from *Pseudomonas aeruginosa*-C1M, characterization and applications as novel multifunctional biocatalyst. BMC Biotechnol. 2025; 25: 27. https://doi.org/10.1186/s12896-025-00959-5.
68. Shitu IG, Katibi KK, Taura LS, Muhammad A, Chiromawa IM, Adamu SB, Iya SGD. X- ray diffraction (XRD) profile analysis and optical properties of Klockmannite copper selenide nanoparticles synthesized via microwave-assisted

© 2025 the authors. This work is licensed under the Creative Commons Attribution 4.0 International License

technique. Ceramics International. 2023; 49(8): 12309-12326. https://doi.org/10.1016/j.ceramint.2022.12.086.

69. Abbas R, Luo J, Qi X, Naz XA, Khan IA, Liu H, Yu S, Wei J. Silver Nanoparticles: Synthesis, Structure, Properties and Applications. Nanomaterials. 2024; 14 (17): 1425. https://doi.org/10.3390/nano14171425.
70. Dekeyrel J, Atkinson R, Chavez E, da-Silva M, Castano OI, Pulleman M, Smolders E. Using optimized monochromatic energy dispersive X-ray fluorescence to determine the cadmium concentration in cacao and soil samples. Heliyon. 2024; 10(20): e39034, https://doi.org/10.1016/j.heliyon.2024.e39034.
71. Karuppannan P, Saravanan K, Egbuna C, Uche CZ, Patrick-Iwuanyanwu KC, Khan J. Antihyperlipidemic Effects of Silver Nanoparticles Synthesized from *Ventilago maderaspatana* Leaf Extract on Streptozotocin-Induced Albino Rats. Trop J Nat Prod Res. 2021; 5 (6): 1066-1071. doi.org/10.26538/tjnpr/v5i6.14.
72. Siddique NA, AL-Samman AM, Kahkashan MA. GC–MS analysis and green synthesis of silver nanoparticles using *Emblica officinalis* leaves and evaluation of its antioxidant and *in-vitro* anti-hypercholesterolemic potential. J Taibah Univ Sci. 2024; 18 (1): 2390211. https://doi.org/10.1080/16583655.2024.2390211.

.

© 2025 the authors. This work is licensed under the Creative Commons Attribution 4.0 International License